Title

Input-Output Functions in Human Heads Obtained With Cochlear Implant and Transcranial Electric Stimulation.

Journal

Neuromodulation : journal of the International Neuromodulation Society, 24(8)

ISSN

1094-7159

Authors

Tran, Phillip
Richardson, Matthew L
Zeng, Fan-Gang

Publication Date

2021-12-01

DOI

10.1111/ner.13065

Peer reviewed

Input-Output Functions in Human Heads Obtained With Cochlear Implant and Transcranial Electric Stimulation

Phillip Tran, PhD [1,*]; Matthew L. Richardson, PhD [1]; Fan-Gang Zeng, PhD [1,*]

[1] Center for Hearing Research, University of California, Irvine, CA, USA

[*] Send correspondence to Phillip Tran and Fan-Gang Zeng, University of California, Irvine, 110 Medical Sciences E, Irvine, CA 92697, USA. Email: phillip.tran@uci.edu (P.T.) and fzeng@uci.edu (F.-G.Z.)

Abstract

Objectives: Electric stimulation is used to treat a number of neurological disorders such as epilepsy and depression. However, delivering the required current to far-field neural targets is often ineffective because of current spread through low-impedance pathways. Here, the specific aims are to develop an empirical measure for current passing through the human head and to optimize stimulation strategies for targeting deeper structures, including the auditory nerve, by utilizing the cochlear implant (CI).

Materials and Methods: Outward input/output (I/O) functions were obtained by CI stimulation and recording scalp potentials in five CI subjects. Conversely, inward I/O functions were obtained by non-invasive transcranial electric stimulation (tES) and recording intracochlear potentials using the onboard recording capability of the CI.

Results: I/O measures indicate substantial current spread, with a maximum of 2.2% gain recorded at the inner ear target during tES (mastoid-to-mastoid electrode configuration). Similarly, CI stimulation produced a maximum of 1.1% gain at the scalp electrode nearest the CI return electrode. Gain varied with electrode montage according to a point source model that accounted for distances between the stimulating and recording electrodes. Within the same electrode montages, current gain patterns varied across subjects suggesting the importance of tissue properties, geometry, and electrode positioning.

Conclusion: These results provide a novel objective measure of electric stimulation in the human head, which can help to optimize stimulation parameters that improve neural excitation of deep structures by reducing the influence of current spread.

Keywords: Transcranial alternating-current stimulation; Cochlear implant; Electroencephalogram; Back-telemetry; Current spread

Conflict of Interest: The authors declare that the research was conducted in the absence of any commercial or financial relationships that could be construed as a potential conflict of interest.

Sources(s) of Financial Support: This work was supported in part by NIH 5 R01 DC015587.

Introduction

Electric stimulation utilizes electric current to excite or inhibit specific structures of the nervous system. It is used to treat a wide variety of neurological disorders including Parkinson's disease[1], epilepsy[2,3], and depression[2,4] through modalities such as deep brain stimulation, vagus nerve stimulation, or transcranial electric stimulation (tES). It is also used to restore motor function for stroke rehabilitation[5] and sensory function such as hearing in the profoundly deaf through the use of a cochlear implant (CI)[6].

The choice of electrode location is important because it, along with the anatomy of the head and the conductive properties of biological tissues[7], gives rise to the resultant electric field and currents in the head, thereby defining the effective activation of target neurons. In general, the current required to excite a neural structure increases with the square of its distance from the stimulating electrode[8–10]. Thus, electrical stimulation is most effective when delivered directly to neural targets through nearby electrodes. Increasing the distance of the electrodes from the target not only decreases the efficiency, it also increases the likelihood of side effects because electric current unavoidably spreads through intermediate tissues including untargeted neurons and receptors[11–13].

For non-invasive/far-field electrode locations used in tES, there is a critical need to empirically monitor electric current passing between the stimulation site and deep neural structures in a living human head. Present methods to characterize current flow from tES are restricted to surface potential recordings with EEG electrodes[14–16], finite-element modelling of the human head[16–21], or voltage distribution within the brains of epilepsy sufferers during surgery[22,23]. These studies showed dominant current shunting through the scalp from tES due to the high resistivity of the skull[19–21]. To produce deep and focal neural stimulation, recent studies have used

electrodes of unique geometries[24], electrodes positioned in strategic locations[25,26], or even simultaneous stimulation from multiple electrodes[16,19]. More recently, the mouse hippocampus was stimulated without activating the overlying cortex through a combination of multiple electrode positions and stimulation waveforms producing temporally interfering patterns[27]. Another study utilized intersectional short pulse stimulation to induce intersecting electric fields by successively building up charge in a region of the mouse brain[28]. Still, focal and deep neural activation by tES remains a challenge.

The present study introduced and experimentally verified a novel method for characterizing current flow during tES by utilizing a neural prosthesis implanted deep within the head—namely, the cochlear implant in the inner ear. Modern CIs can not only deliver current to the deafened ear to restore hearing but also record voltages in the inner ear through a recording circuit embedded in the cochlear implant (i.e. back-telemetry)[29,30]. This dual-capacity technology offers a unique opportunity to either deliver or record stimuli from within a deep region of the head (**Figure 1**). First, we used CI stimulation and scalp recordings to characterize the "outward" input/output (I/O) function[23,31]. Second, we used tES and CI recordings to characterize the "inward" I/O function. Third, we investigated the effects of phase duration and current intensity on the recordings[16,23,32], and derived an analytical model to fit these I/O functions. Finally, we discussed potential methods to advance this novel technique and improve the depth and focality of tES.

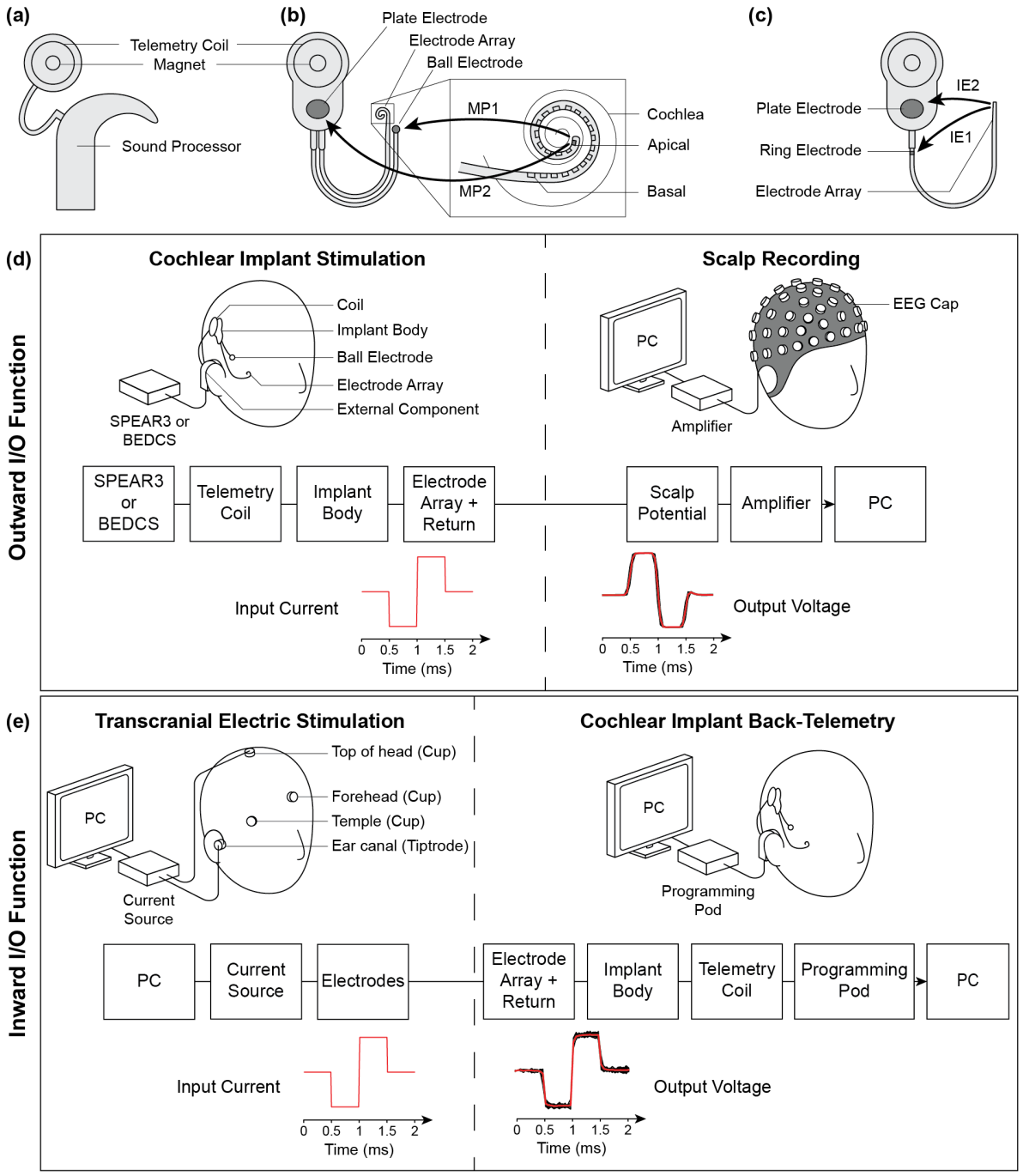

Figure 1. (a) External component of a cochlear implant system that is worn over the ear. (b) Internal component of a Nucleus cochlear implant with close up of the electrode array inserted into the cochlea. Stimulation is between the apical electrode and the ball (MP1) or plate (MP2) electrode. (c) Internal component of a HiRes 90K cochlear implant. Stimulation is between the apical electrode (not shown) and the ring (IE1) or plate (IE2) electrode. (d) Outward I/O functions obtained by delivering current to the inner ear via cochlear implant stimulation and recording scalp potentials via EEG electrodes. (e) Inward I/O functions obtained by delivering current to the head via a pair of electrodes at locations including the ear canals, mastoids, temples, forehead, top of the head, and nape (some locations not shown) and recording potentials at the inner ear via cochlear implant back-telemetry.

Material and Methods

Subjects

Five cochlear implant recipients, aged between 49 and 78 years, participated in the study (**Table 1**). Subject 1 (S1) was a bilateral user and was only tested on one side. All the other subjects were unilateral users. The cochlear implant is comprised of an external component that is worn behind the ear which communicates wirelessly with the internal component via telemetry (**Figure 1**(a)). S1-S4 were users of the Nucleus implant device (Cochlear Ltd., Sydney, Australia), namely the Nucleus 24, Freedom, or CI512, with an intracochlear electrode array consisting of 22 electrodes (**Figure 1**(b)). S5 used the HiRes 90K implant (Advanced Bionics, Valencia, CA, USA) with an array consisting of 16 electrodes (**Figure 1**(c)). Each subject provided their radiological scans for analysis of head dimensions and implant location (**Figure 2**). The experimental protocol was approved by the University of California, Irvine Institutional Review Board and all subjects gave written informed consent to participate in the study.

Table 1. Subject Demographics and Current Amplitude(s) Used in CI Stimulation and tES Studies.

						Current Amplitude (μA)		
ID	**Gender**	**Age**	**Uni- / Bi-lateral**	**Tested Ear**	**Device**	**CI Stim (100 μs)**	**CI Stim (500 μs)**	**tES**
S1	F	56	Bilateral	R	Nucleus 24	20, 27, 31, 57	20, 27, 31	50
S2	M	50	Unilateral	R	Nucleus Freedom	N/A	20, 27, 31	150
S3	F	49	Unilateral	L	Nucleus Freedom	20, 27, 57	20, 27	100
S4	F	67	Unilateral	L	Nucleus CI512	N/A	N/A	400
S5	M	78	Unilateral	R	HiRes 90K	20, 75, 120	N/A	100

M/F, Male/Female; R/L, Right/Left.

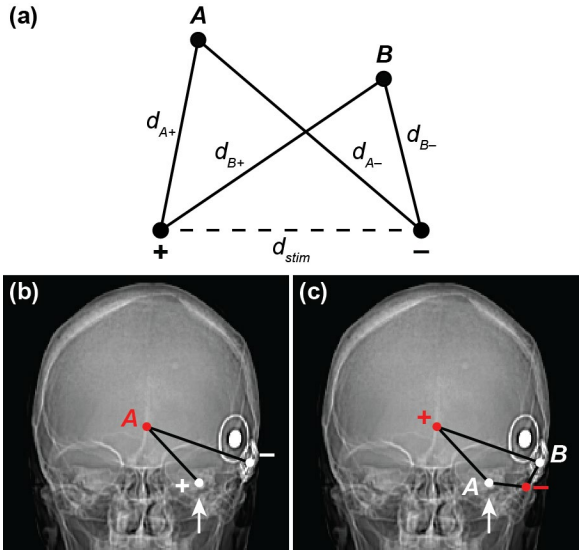

Figure 2. (a) A pair of point charges are used to model a pair of stimulating electrodes. The electric potential at a target *A* and reference *B* is determined by their distance from the active ('+') and return ('–') electrodes (d_{A+} and d_{A-}, and d_{B+} and d_{B-}, respectively). d_{stim} represents the distance separating the two electrodes. (b),(c) X-ray of S4 with external electrode positions (red points), internal cochlear implant (white components), and intracochlear electrode array (white arrow) with labels corresponding to points in (a). (b) Outward I/O recording: locations of CI stimulating electrodes with an example of a single recording site *A* on the scalp. The reference *B* is located on the knee (not shown). (c) Inward I/O recording: same as (b), but with the intracochlear electrode as recording site *A* and the monopolar return electrode as reference *B*.

Cochlear Implant Stimulation

The outward I/O function was measured by delivering electric stimuli through the cochlear implant and measuring the outward-going voltage potentials on the scalp (**Figure 1**(d)). All stimuli consisted of charge-balanced biphasic pulses with phase durations of 100 or 500 µs delivered from the most apical intracochlear electrode at a pulse rate of 500 Hz. The stimulus intensity was set up to 4 levels, between 20 and 120 µA, ranging from below the subject's auditory threshold to a comfortable loudness level (**Table 1**) and was delivered continuously for approximately 90 seconds. Due to time restrictions, S2 only participated with 500 µs phase duration stimuli here, and S4 did not participate in this part of the study.

For the Nucleus subjects, a Sound Processor for Electrical and Acoustic Research (SPEAR3, HearWorks Pty. Ltd., Melbourne, Australia) was connected to the CI processor to control stimulus delivery[33]. Two CI return modes were tested: MP1 (remote ball electrode) and MP2 (plate electrode on the CI case) (**Figure 1**(b)). Stimulus level was controlled by an analog dial with positions corresponding to standard clinical units, which enabled the conversion to electric current. For the HiRes subject, electric stimuli were controlled by the Bionic Ear Data Collection System software (BEDCS v1.17.208, Advanced Bionics, Valencia, CA)[34,35]. Due to limitations of this software, only a phase duration of 100 μs was used. Two CI return modes were tested: IE1 (ring electrode near the CI case) and IE2 (plate electrode on the CI case) (**Figure 1**(c)). The computer was connected to the subject's CI device via a programming pod to deliver the stimulus, with stimulus level being controlled through the software.

Scalp potentials were recorded using the Neuroscan SynAmp2 system and Scan 4.5 software with either a QuikCap 32-channel or 64-channel cap (SynAmps2, Compumedics Neuroscan, Charlotte, NC, USA). Electrode locations were determined by the standard 10–20 system including intermediate positions and a neutral reference electrode was placed on the knee. Contact with the skin could not be achieved for two scalp electrodes over the CI telemetry coil (CP5/TP7 for left CI users, CP6/TP8 for right CI users), so these were excluded from the recording. Subjects were seated comfortably and asked to remain still during recordings.

All raw waveforms were captured at 20 kHz sampling frequency with a 3.5 kHz antialiasing filter and the recordings were averaged over 120 stimulus presentations for analysis. The peak amplitude of the leading waveform phase was determined and used for all comparisons in this study.

The impedance between the stimulating electrodes was determined using Custom Sound EP (Cochlear Ltd., Sydney, Australia) for Nucleus and SoundWave (Advanced Bionics, Valencia, CA, USA) for HiRes. To enable conversion of this value to input voltage through Ohm's law, the capacitive component of the impedance was calculated via an analytical model derived by Dual et al.[36] and then subtracted from the impedance measurement. Here, 5000 and 1000 Hz frequencies were used for the 100 and 500 μs phase duration biphasic square pulses, respectively.

Transcranial Electric Stimulation

The inward I/O function was measured by delivering an electric stimulus through transcranial scalp electrodes and measuring the inward-going voltages with the CI "back-telemetry" recording circuit (**Figure 1**(e)). As with CI stimulation, all stimuli were charge-balanced biphasic pulse trains at a pulse rate of 500 Hz with either 100 or 500 μs phase duration. The electric stimulus was delivered continuously at a single current level set below the subject's sensation threshold (**Table 1**) for approximately 90 seconds.

The stimulus was generated digitally using Matlab (R2015a, Mathworks, Natick, MA, USA) and delivered via a soundcard to a custom-built constant-current source. Prior to each experiment, the system was calibrated to a maximum output of 2 mA by connecting a 1 kΩ resistor and measuring output voltage on an oscilloscope. During the experiment, the resistor was disconnected, and current-controlled stimulation was delivered to a pair of electrodes ("active" and "return") on the subject's head. The oscilloscope was used here to monitor the input voltage between the two electrodes during the stimulation. For safety, stimulation was only delivered when both the subject and experimenter each compressed their own foot-pedal and was stopped

immediately when either pedal was released. The subject was isolated from direct connection to mains with a transformer power supply.

Transcranial electric stimulation was delivered using electrode pairs that included locations in the ear canals (ipsilateral and contralateral to the CI), mastoids, temples, forehead, top of the head, and nape. For the ear canal location, a gold-foil-wrapped-foam tiptrode (Etymotic ER3-26A, Elk Grove Village, IL, USA) coated with conductive gel (SignaGel, Parker Laboratories, Inc., Fairfield, NJ, USA) was used. The electrode was inserted with a maximum insertion depth of 2 cm from the ear canal opening. All other locations utilized a gold cup electrode (Natus Neurology-Grass, Warwick, RI, USA) adhered to the skin with electrode cream (EC2 Electrode Cream, Natus Neurology-Grass).

Voltages were recorded using the respective CI manufacturer's neural response back-telemetry program: Custom Sound EP 3.2 for Nucleus subjects and SoundWave for the HiRes subject. First, the subject's CI was connected to the computer via an external programming pod. Next, electric stimulation was delivered to the subject while simultaneously recording voltages at the most apical CI electrode with reference to the MP1 or IE1 electrode at 20 or 28 kHz sampling frequency, respectively, using a 10 kHz antialiasing filter. 52 raw waveforms were processed to create an average waveform and the peak amplitude was determined for all the comparisons in this study.

Gain Model

A simple model was derived to predict the expected gain for any given pair of stimulating electrodes. The model assumes that the stimulating electrodes are a pair of point current sources in a homogeneous medium based on the quasi-static approximation with electrodes that are small

compared to the domain space[37]: the active electrode is modeled as a positive current source while the return electrode is modeled as a negative current source (**Figure 2**(a)).

For any single current source, the electric potential *V* at any point *A* can be determined using:

$$V_A = \frac{I}{4\pi\sigma d} \quad \textbf{(1)}$$

where *I* is the current level, *d* is the distance between point *A* and the source, and σ is the effective conductivity of the medium[37]. When more than one source is present, the net electric potential at *A* is the sum of the electric potentials from each individual source, as defined by the principle of superposition. For a system with two equal and opposite sources ($I = I_+ = -I_-$), the electric potential at *A* becomes:

$$V_{rec} = V_A = \frac{I_+}{4\pi\sigma d_{A+}} + \frac{I_-}{4\pi\sigma d_{A-}} = \frac{I}{4\pi\sigma}\left(\frac{1}{d_{A+}} - \frac{1}{d_{A-}}\right) \quad \textbf{(2)}$$

where d_{A+} and d_{A-} are distances between *A* and the positive and negative sources, respectively. For CI stimulation, point *A* represents a scalp recording electrode, and the two sources represent the intracochlear electrode and monopolar return (**Figure 2**(b)).

For tES, stimulating scalp electrodes deliver current from the skin surface into the head. This can be represented as point current sources on a half-space domain, effectively doubling the voltage that is generated compared to an electrode embedded within a full-space domain. Additionally, CI back-telemetry measures electric potential as the potential difference between the recording intracochlear electrode (point *A*) and the reference monopolar electrode (point *B*) (**Figure 2**(c)). From these, the voltage is:

$$V_{rec} = V_A - V_B = \frac{I}{2\pi\sigma}\left[\left(\frac{1}{d_{A+}} - \frac{1}{d_{A-}}\right) - \left(\frac{1}{d_{B+}} - \frac{1}{d_{B-}}\right)\right] \quad \textbf{(3)}$$

The voltage gain, *G*, is defined as the ratio of the output voltage to the input voltage. This forms the following two proportionalities for CI stimulation and tES, respectively:

$$G_{CIStim} = V_{rec}/V_{stim} = \frac{I}{4\pi k}\left(\frac{1}{d_{A+}} - \frac{1}{d_{A-}}\right) \quad \textbf{(4)}$$

$$G_{tES} = V_{rec}/V_{stim} = \frac{I}{2\pi k}\left[\left(\frac{1}{d_{A+}} - \frac{1}{d_{A-}}\right) - \left(\frac{1}{d_{B+}} - \frac{1}{d_{B-}}\right)\right] \quad \textbf{(5)}$$

where $k = \sigma V_{stim}$, an arbitrary constant with units VSm^{-1} that is to be determined to produce the best fit for *G* with the experimental data. Distances between electrodes were determined through post-op CT scans provided by the subjects for internal CI electrodes, and by scaling the standard EEG locations files for the QuikCap (Neuroscan) by each subject's head-size for external scalp electrodes.

Results

Cochlear Implant Stimulation and Scalp Recordings

Typical raw scalp recordings from CI stimulation are shown in **Figure 3**(a),(b) as average waveforms. Only a few of the recording sites near the cochlear implant return electrode exhibited large voltage magnitudes of 3 mV (signal-to-noise ratio = 48.1 dB), with potential dropping off sharply away from these sites. The noise level was measured as the root-mean-squared voltage between pulses and was found to be 10.3 ± 6.4 μV for all raw waveforms and 1.1 ± 0.9 μV after averaging within a dataset.

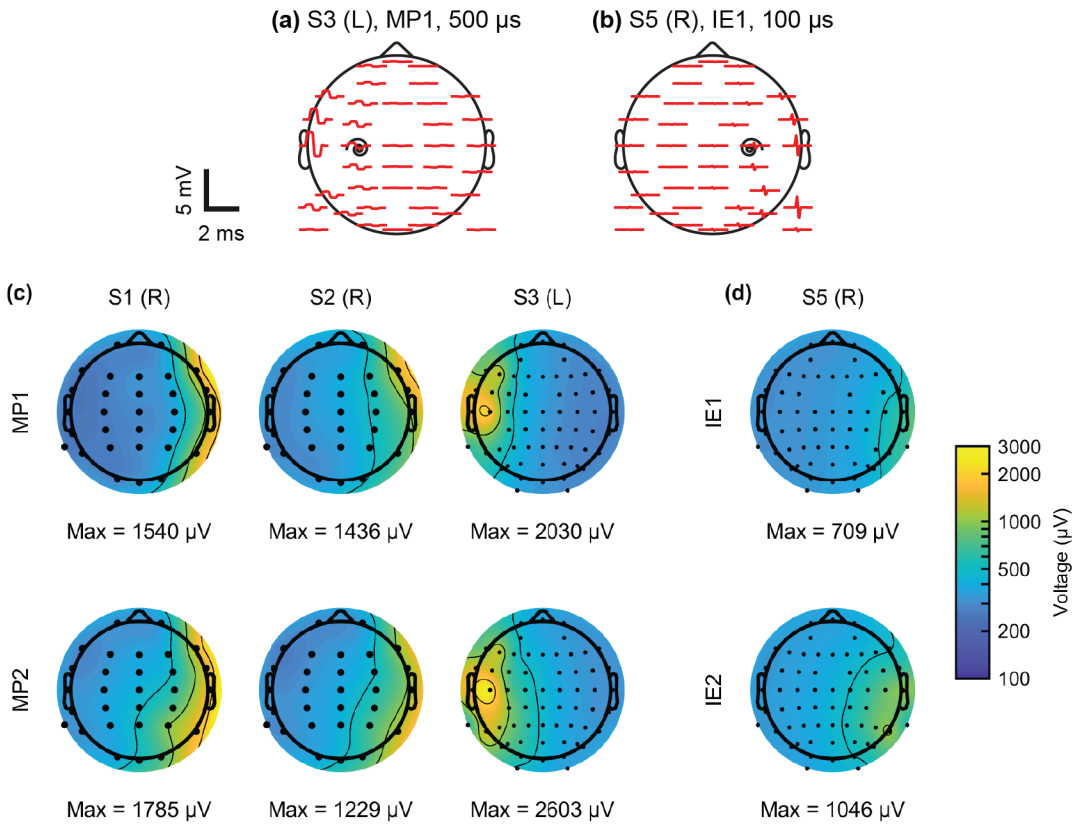

Figure 3. (a),(b) Representative scalp recordings from the 64-electrode site EEG cap due to cochlear implant stimulation for subjects S3 (MP1, 500 µs phase duration) and S5 (IE1, 100 µs phase duration), respectively, at 20 µA. (c),(d) Topographic maps obtained from scalp recordings of CI stimulation for MP1 and MP2 stimulation (S1, S2, and S3), and IE1 and IE2 stimulation (S5) after correcting for the bias of the reference electrode. Topographies represent the peak amplitude of the leading waveform phase. A logarithmic color scale was utilized. Contour lines were placed at 100, 200, 500, 1000, and 2000 µV. L/R, Left/Right cochlear implant.

Negative or reverse-polarity potentials were observed on the contralateral side of stimulation, indicating a bias in the recordings. A finite element model of the human head created for CI stimulation[38] was used to estimate the bias, and this value was subsequently subtracted from all recordings. Topographic maps are shown with a logarithmic color scale for four subjects at 20 µA stimulus current for ease of visualization and comparison (**Figure 3**(c),(d)). First, voltage depends highly on CI side, with peak potentials on the right side for S1, S2, and S5, and on the left side for S3. Second, voltage distribution also depends on the CI return electrode, with peak potentials centered around the temporal region for MP1 stimulation, and more posteriorly for

MP2 stimulation (Nucleus users S1-S3). Peak potentials were located posterior to the ear for the HiRes user, with the IE1 peak location being inferior/lateral to that of IE2. Third, voltage distributions were different between subjects in terms of peak value and location, indicating individual head variability as well as individual differences in the placement of the return electrode or implant body.

Transcranial Electric Stimulation and Cochlear Implant Recordings

Forty different electrode pair configurations were tested for tES. Select averaged waveforms for two subjects are shown in **Figure 4**. First, voltage magnitudes recorded by back-telemetry were highly dependent on the location of the stimulating electrodes relative to the CI recording electrodes. Near-zero voltages were more likely when both stimulating electrodes were either close to the recording electrodes, such as the ipsilateral ear canal and mastoid (Ei-Mi), or far away from the CI recording electrodes, such as the top of the head and forehead (Cz-Fpz). On the other hand, large voltage magnitudes of up to 3.5 mV were recorded when only one of the stimulating electrodes was close to the recording electrodes, for example, the ipsilateral and contralateral ear canal (Ei-Ec) and mastoid (Mi-Mc) configurations. Second, the polarity of the voltage waveform was dependent on which of the two stimulating electrodes was used as the "active" or positive site. Switching the active and return sites for an electrode configuration reversed the polarity of the recording (Mi-Mc vs Mc-Mi). Third, voltage magnitudes varied between subjects for the same stimulating electrode pair and input current, indicating differences in head anatomy and the placement of the electrodes.

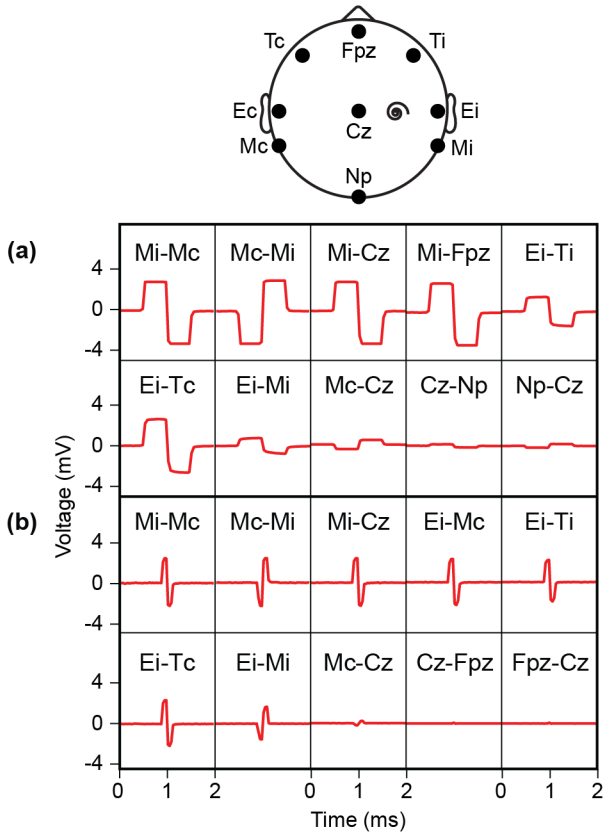

Figure 4. Cochlear implant back-telemetry recordings from individual scalp stimulation pairs during transcranial electric stimulation for: (a) S3 (500 µs phase duration), and (b) S5 (100 µs phase duration), respectively. Above each waveform is the pair of electrodes used for stimulation, written as "active"-"return". Head schematic shows electrode locations for a right CI subject. C, contralateral; Cz, top of head; E, ear canal; Fpz, forehead; i, ipsilateral; M, mastoid; Np, nape; T, temple.

Effect of Phase Duration

Figure 5 compares the measured voltages for 100 and 500 µs phase duration stimuli during both CI stimulation and tES. For CI stimulation, voltages at 100 µs phase duration were 14% lower than those at 500 µs (**Figure 5**(a), $r = 0.983$, $n = 386$, $p < 0.001$). The deviation can be explained by: (1) the transient effects of the electrode-electrolyte interface of the CI electrodes giving rise to larger voltages for longer pulses[39], and (2) the low cutoff frequency for the antialiasing filter preventing the waveform from reaching its peak for the 100 µs signal. Results for the two phase durations were more similar for tES, with the 100 µs phase duration electric potentials being

only 4% lower than for 500 µs (**Figure 5**(b), $r = 0.999$, $n = 98$, $p < 0.01$). Based on the high correlation of these data and the assumption of linear resistive behavior in the head, the electric potentials for 100 µs phase duration were scaled by 1.16 (for CI stimulation) and 1.04 (for tES) for the following results sections.

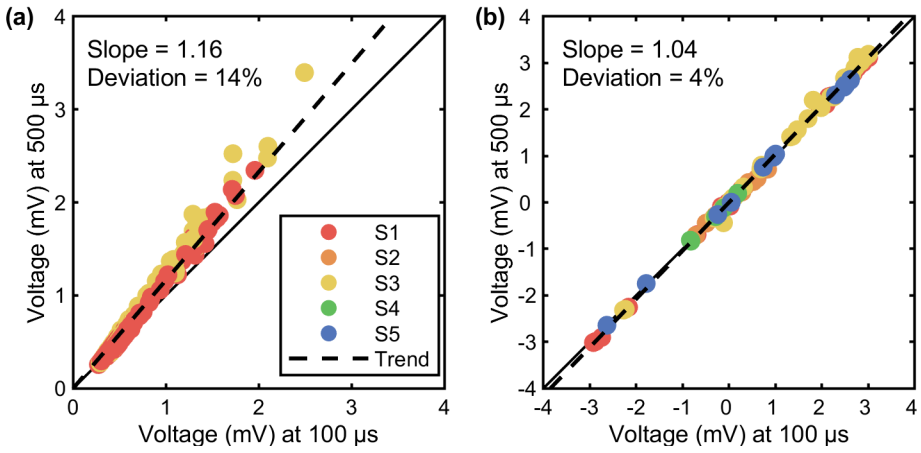

Figure 5. (a) Comparison of voltages obtained using 100 and 500 µs phase duration for CI stimulation. S2 was presented with only 500 µs pulses, and S5 with 100 µs pulses. S4 did not participate. (b) Comparison of voltages obtained using 100 and 500 µs phase duration for tES. All 5 subjects were presented with both phase durations.

Effect of Current Input

The effect of input current intensity on the output voltage was investigated for CI stimulation and the results are shown for each dataset (subject and phase duration combination) in **Figure 6**. Input current was normalized to the largest current value for a dataset (reported in **Table 1**) to enable comparison between subjects. Output voltage at each recording location was normalized to the scalp potential recorded using the highest stimulation level to enable comparison between locations and individuals. Each point represents the average and standard deviation across recording locations for one dataset at a single current level. As expected, scalp potential increased with increasing current for all subjects, with a highly significant linear fit across all test

conditions (slope = 1.02, r = 0.95, n = 1247, $p < 0.001$) suggesting that the electric stimulation I/O function is linear in the human head.

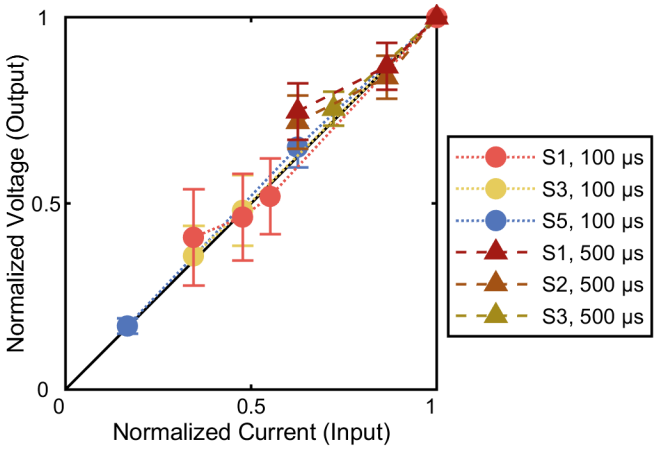

Figure 6. Input-output plot for cochlear implant stimulation for different datasets. A dataset refers to a subject being stimulated using a selected phase duration as reported in **Table 1**. The input current was normalized to the largest current value used for any dataset. For any recording site in a dataset, the output voltage was normalized to the voltage obtained with the largest current for that dataset. Points and error bars represent the mean and standard deviation of the normalized voltages over all the recording sites for a single current level.

Gain

Figure 7 shows the experimental gain for both CI stimulation and tES. As plotted on the y-axis, gain measured from CI stimulation (**Figure 7**(a)) ranged from 0.12% to 1.1%, with the maximum measured at the scalp electrode nearest the CI return. For tES (**Figure 7**(b)), the gain ranged from -2.2% to 2.1%, with the maximum magnitude obtained from the ipsilateral to contralateral mastoid electrode pair (Mi-Mc). Second, substantial current spread was present in both outward and inward stimulation, with only 22% of tES electrode pair configurations producing a gain greater than 1%, and only one scalp recording site reaching this gain for CI stimulation. Third, the value for k was determined for each individual as a fitting parameter for the point source model of gain (x-axis, **Figure 7**). k values are listed in **Table 2** and was found to be 0.078 ± 0.008 VSm^{-1} for CI stimulation and 0.151 ± 0.030 VSm^{-1} for tES. For CI stimulation,

gain varied as a function of electrode montage according to two distances (**Equation 4**): active stimulating to the target recording electrode and return stimulating to the target recording electrode (**Figure 7**(a)). The gain for tES also varied with electrode montage but required the knowledge of two additional distances (see **Equation 5**): active stimulating to monopolar reference electrode and return stimulating to monopolar reference electrode (**Figure 7**(b)).

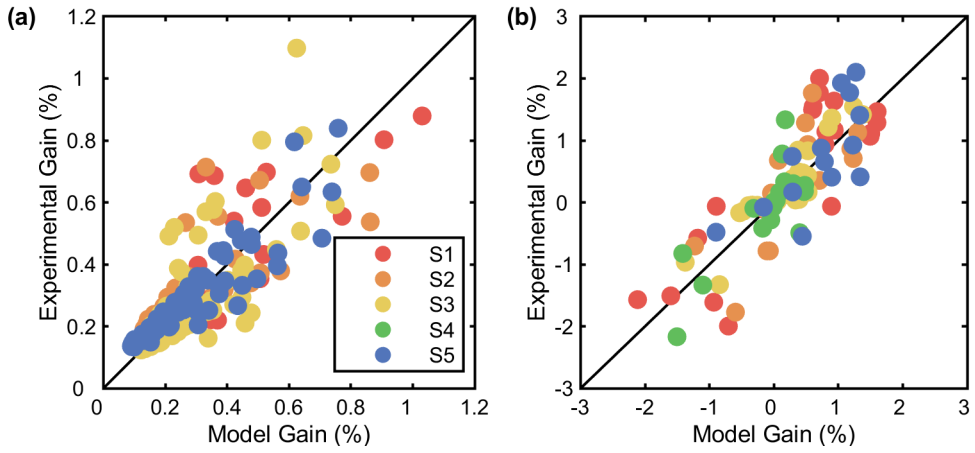

Figure 7. Experimental gain plotted against model gain. (a) For CI stimulation, experimental gain was the ratio of the recorded scalp potential and the stimulation voltage (calculated from impedance and input current). Model gain was fitted using **Equation 4**. (b) For tES, experimental gain was the ratio of the recorded voltage by back-telemetry and the stimulation voltage (recorded via the oscilloscope). Model gain was fitted using **Equation 5**.

Table 2. Gain Model Fit Constant, *k*, and Correlation Coefficient, *r*, for CI Stimulation and tES.

	CI Stim (20 µA)		**tES (100 µA)**	
ID	***k***	***r***	***k***	***r***
S1	0.070	0.885	0.186	0.846
S2	0.073	0.854	0.136	0.733
S3	0.088	0.817	0.165	0.904
S4	-	-	0.108	0.793
S5	0.081	0.936	0.159	0.745

Discussion

The present study delivered electric stimulation to the human head in both outward and inward directions, namely cochlear implant stimulation and transcranial electric stimulation, while recording their resulting electric potentials using scalp electrodes and cochlear implant back-telemetry, respectively. Summarizing the main results here: (1) the voltage recording magnitude and polarity for both outward and inward stimulation are dependent on the location and distance of the recording electrodes from the stimulating electrodes; (2) voltage increases due to transient effects at the electrode-electrolyte interface are present for pulsed stimuli; (3) recordings are linearly dependent on current amplitude; (4) maximum gain was only 2.2%; and (5) a point current source model can predict the gain based on distances between electrodes.

Technology Advantages and Limitations

To our knowledge, this is the first study that utilizes cochlear implant back-telemetry to record electric potentials resulting from electric stimulation other than the CI itself. Using the CI in this way provides a recording device that is permanently inside the living human head. This has two benefits: (1) not having to use animal models in place of human subjects, and (2) avoiding the need for surgical methods to temporarily insert intracranial recording electrodes. A potential limitation is that the presence of the CI in the head can distort the tES electric field in the vicinity of the components, affecting the reliability in extrapolating these results to non-CI subjects. Nevertheless, we can take advantage of this device in subjects to measure the gain in the inner ear and approximate the proportion of stimulating current reaching the auditory nerve during tES.

The present study utilizes an EEG cap for the measurement of scalp potentials resulting from CI stimulation, however not all EEG electrode sites could be used. Most of the unused electrodes

were in the vicinity of the implant body because the external coil prevented some electrodes from contacting the skin. If these electrodes could be included, it is expected that they would record higher electric potentials than those reported in this study, and therefore increase the maximum gain, especially for stimulation modes like MP2 and IE2 where the return electrode is on the implant body. In addition, the location of the reference electrode for the scalp potentials produced a bias in the recordings. The bias potential determined from the finite element model only represents an approximation and would need to be validated experimentally. Ideally, both the CI stimulation and scalp recording setups would utilize the same reference electrode to capture the true potentials without any bias.

An analytical model of impedance was used to determine the capacitive component of impedance in this study[36]. However, this has some drawbacks. First, the model was based on CI stimulation in an animal model using an electrode array designed for cats. Here, we assume that the electrode surface area is similar to that used in a typical human CI. Differences in impedance were observed between different cats and also between individual electrodes on an array, suggesting variations in anatomy, electrode position, and fibrous tissue formation around the electrode play a key role in changing the impedance near an electrode. This has implications on our study as each subject needs to be considered on an individual basis, however, the same capacitive impedance value was used for all subjects. Finally, only one frequency component was used to approximate the biphasic square pulse. Knowing additional frequency terms here can provide a more accurate solution.

Electric Stimulation I/O Functions

For CI stimulation, polarization at the electrode-electrolyte interface likely gave rise to larger voltages for pulses with longer phase duration. This has been well studied by others for various

electrode geometries[39], size[40], and surface types and materials[41]. The complex geometry and environment here for the cochlear implant makes it difficult to determine the transition time between stimulus onset and steady-state conditions. The use of surface electrodes for tES has a different effect with voltages depending more on the location than the surface contact.

Linear resistive behavior of the head was observed for CI stimulation, agreeing with the findings of experimental and modeling studies on electric stimulation[16,23,32] and **Equation 1**[37]. Knowing this permits estimation of the resulting voltage and electric fields for both outward and inward stimulation modalities by scaling. However, simply increasing the current delivered will not solve the deep-targeting problem due to safety concerns[40,42], so the question becomes focusing the current toward the target site.

The maximum gain obtained from all test cases was only 2.2%, suggesting only a small amount of current was able to reach the inner ear target. This is expected due to the location of the stimulating electrodes and their distance from the target site. The recorded gain, together with the model results, highlights the challenge in activating deep neural targets non-invasively, particularly the auditory nerve inside the densest bone in the skull. Unfortunately, even if the stimulating electrodes are positioned closer to the target neurons, current spread is still present through low impedance pathways. For example, CI stimulation of auditory nerve fibers often results in shunting along the length of the cochlea when monopolar mode is used[43,44]. Moreover, the two stimulation cases differ in the tissue volume surrounding the stimulating electrodes, with current being delivered into a half-space domain for tES and a full-space domain for CI stimulation. This is likely to explain the doubling of gain for the inward stimuli compared to the outward scenario.

Finding ways to increase the amount of current reaching deep target structures remains an important goal for achieving more effective stimulation with remote electrodes. One method is to steer the current in the direction of the target by optimizing the locations of the stimulating electrodes. From **Equation 5**, the relative distances of the stimulating electrodes to the recording electrodes determine the gain. Our results showed that having one of the stimulating electrodes close to the target site while having the other electrode on the opposite side of the head produced the largest gain magnitude and increased the current traveling to the target[45]. As examples, the ipsilateral and contralateral ear canal (Ei-Ec) or the ipsilateral mastoid and forehead (Mi-Fpz) electrode pair both exhibited large gains for the intracochlear target. The orientation of the electrodes in space is also important as it affects the distances between the electrodes. While these values were obtained with only a single pair of electrodes, there is potential to further increase the focality of the stimulation by employing additional electrodes in novel arrangements with optimized input currents[19,46] and waveforms[27].

Within the same electrode montages for tES, current gain patterns varied across subjects suggesting the importance of tissue properties, geometry, and electrode positioning[47]. For brain stimulation, factors such as head size, skull thickness[45], or muscle tissue thickness may contribute to inter-individual differences[22]. This variation between subjects suggests that stimulation parameters for tES would need to be catered for each subject if it was to be used clinically, agreeing with recommendations by others[22]. Once an ideal configuration is found for a particular subject, an extra step of fine-tuning can be performed to achieve the best result.

Far-Field Modeling

The gain fitting model used in this study was made based on a few assumptions. First, the derivation assumed the stimulating electrodes to be charged current sources. Realistically, the

electrodes have differing size and shape, which can produce non-uniform distributions near the surface and affect the amount of current passing through different tissues. Second, the model assumes a homogeneous medium, which greatly differs from what is present in a human head with a wide range of tissues, each possessing differing electric conductivity. The skull is a highly resistive tissue that can prevent current from reaching an auditory nerve target. The fitting parameter determined in this model varied between individuals, which is likely to be explained by the above points. Regardless, the model still provided a reliable means for verifying the gain for CI stimulation and tES with correlation coefficients above 0.73 (**Table 2**) and approximating the amount of current reaching a target. While activation of a neuron or brain region is better defined by electric field or current density, it is difficult to obtain these measures *in vivo*. Computational modeling methods, such as finite element modeling for volume conduction and neural modeling for activation[48], can be used to fill this space and further optimize electric stimulation techniques across a wide variety of applications, including deep brain stimulation[49,50], vagus nerve stimulation[51], and CI stimulation[32,38]. In turn, the electric potential data presented here can serve as a unique validation method to ensure such models are reliable in their predictions.

Implications

Deep neural targets, such as the thalamus, vagus nerve, or auditory nerve, remain challenging targets for electric stimulation for the reasons mentioned above. However, they remain important targets for non-invasive stimulation. To date, non-invasive deep brain stimulation has not been achieved in humans. However, remote activation of the auditory nerve through tES has been shown to produce auditory sensations[26,52], suppress the loudness of tinnitus[25,26,52,53], and reduce the annoyance of the tinnitus[53]. Optimizing stimulation parameters with the methods introduced

here, could aid the development of viable treatment or therapy options for a wide variety of neurological disorders. These techniques can also be extended to other chronically implanted devices, including those used in deep brain stimulation or vagus nerve stimulation, to study how transcranial currents reach other deep neural targets and, in turn, how their electrical artifacts pass through the head.

Conclusions

In this study, we measured electric potentials resulting from CI stimulation and tES to better understand the spreading of current from various electrode montages. We found large amounts of current spread for tES, with a maximum gain of only 2.2%. Variations were observed between subjects for the same stimulation configuration, suggesting stimulation parameters should be made patient-specific. The techniques described here can enable us to optimize these stimulation parameters to activate deep targets non-invasively, such as the auditory nerve, and improve tES strategies for treating neurological disorders.

Conflict of Interest

The authors declare that the research was conducted in the absence of any commercial or financial relationships that could be construed as a potential conflict of interest.

Acknowledgements

The authors thank the four anonymous reviewers for their comments which have greatly improved the manuscript.

Authorship Statements

The authors declare that each person listed as an author has contributed sufficiently in the work including the concept and design, data collection, analysis, and writing of the manuscript. Fan-Gang Zeng was responsible for the study concept and design. Matthew L. Richardson was responsible for data collection. Phillip Tran and Matthew L. Richardson were responsible for data analysis. Phillip Tran, Matthew L. Richardson, and Fan-Gang Zeng wrote the manuscript. All authors have approved the final version of the manuscript.

References

1. Benabid AL, Chabardes S, Mitrofanis J, Pollak P. Deep brain stimulation of the subthalamic nucleus for the treatment of Parkinson's disease. *Lancet Neurol*. 2009;8:67-81. doi:10.1007/s00701-009-0293-6

2. Howland RH. Vagus nerve stimulation. *Curr Behav Neurosci Reports*. 2014;1(2):64-73. doi:10.1007/s40473-014-0010-5

3. Berényi A, Belluscio M, Mao D, Buzsáki G. Closed-Loop Control of Epilepsy by Transcranial Electrical Stimulation. *Science (80-)*. 2012;337(6095):735-737. doi:10.1126/science.1223154

4. Fregni F, Boggio PS, Nitsche MA, Marcolin MA, Rigonati SP, Pascual-Leone A. Treatment of major depression with transcranial direct current stimulation. *Bipolar Disord*. 2006;8:203-204. doi:10.1007/s00134-003-2126-z

5. Peckham PH, Knutson JS. Functional Electrical Stimulation for Neuromuscular Applications. *Annu Rev Biomed Eng*. 2005;7(1):327-360.

doi:10.1146/annurev.bioeng.6.040803.140103

6. Clark GM. *Cochlear Implants: Fundamentals and Applications*. (Beyer RT, ed.). New York: Springer-Verlag; 2003.

7. Salvador R, Ramirez F, V'yacheslavovna M, Miranda PC. Effects of tissue dielectric properties on the electric field induced in tDCS: a sensitivity analysis. In: *34th Annual International Conference of the IEEE Engineering in Medicine and Biology Society*. San Diego, California, USA; 2012:787-790. doi:10.1109/embc.2012.6346049

8. Ranck, Jr. JB. Which elements are excited in electrical stimulation of mammalian central nervous system: a review. *Brain Res*. 1975;98:417-440. doi:10.1016/0006-8993(75)90364-9

9. Bagshaw E V., Evans MH. Measurement of current spread from microelectrodes when stimulating within the nervous system. *Exp Brain Res*. 1976;25(4):391-400. doi:10.1007/BF00241729

10. Brocker DT, Grill WM. *Principles of Electrical Stimulation of Neural Tissue*. Vol 116. 1st ed. Amsterdam, Netherlands: Elsevier B.V.; 2013. doi:10.1016/B978-0-444-53497-2.00001-2

11. Brunoni AR, Amadera J, Berbel B, Volz MS, Rizzerio BG, Fregni F. A systematic review on reporting and assessment of adverse effects associated with transcranial direct current stimulation. *Int J Neuropsychopharmacol*. 2011;14(8):1133-1145. doi:10.1017/S1461145710001690

12. Matsumoto H, Ugawa Y. Adverse events of tDCS and tACS: A review. *Clin Neurophysiol*

Pract. 2017;2:19-25. doi:10.1016/j.cnp.2016.12.003

13. Zeng F-G, Tran P, Richardson M, Sun S, Xu Y. Human Sensation of Transcranial Electric Stimulation. *Sci Rep*. 2019;9(15427):1-12. doi:10.1038/s41598-019-51792-8

14. Roy A, Baxter B, He B. High-definition transcranial direct current stimulation induces both acute and persistent changes in broadband cortical synchronization: A simultaneous tDCS-EEG study. *IEEE Trans Biomed Eng*. 2014;61(7):1967-1978. doi:10.1109/TBME.2014.2311071

15. Law SK. Thickness and resistivity variations over the upper surface of the human skull. *Brain Topogr*. 1993;6(2):99-109. doi:10.1007/BF01191074

16. Datta A, Zhou X, Su Y, Parra LC, Bikson M. Validation of finite element model of transcranial electrical stimulation using scalp potentials: implications for clinical dose. *J Neural Eng*. 2013;10(3):036018. doi:10.1088/1741-2560/10/3/036018

17. Kwon OI, Sajib SZK, Sersa I, et al. Current Density Imaging During Transcranial Direct Current Stimulation Using DT-MRI and MREIT: Algorithm Development and Numerical Simulations. *IEEE Trans Biomed Eng*. 2016;63(1):168-175. doi:10.1109/TBME.2015.2448555

18. Huang Y, Parra LC. Can transcranial electric stimulation with multiple electrodes reach deep targets? *Brain Stimul*. 2019;12(1):30-40. doi:10.1016/j.brs.2018.09.010

19. Dmochowski JP, Datta A, Bikson M, Su Y, Parra LC. Optimized multi-electrode stimulation increases focality and intensity at target. *J Neural Eng*. 2011;8(4):046011. doi:10.1088/1741-2560/8/4/046011

20. Miranda PC, Lomarev M, Hallett M. Modeling the current distribution during transcranial direct current stimulation. *Clin Neurophysiol*. 2006;117(7):1623-1629. doi:http://dx.doi.org/10.1016/j.clinph.2006.04.009

21. Neuling T, Wagner S, Wolters CH, Zaehle T, Herrmann CS. Finite-element model predicts current density distribution for clinical applications of tDCS and tACS. *Front Psychiatry*. 2012;3(SEP):1-10. doi:10.3389/fpsyt.2012.00083

22. Opitz A, Falchier A, Yan CG, et al. Spatiotemporal structure of intracranial electric fields induced by transcranial electric stimulation in humans and nonhuman primates. *Sci Rep*. 2016;6(March):1-11. doi:10.1038/srep31236

23. Huang Y, Liu AA, Lafon B, et al. Measurements and models of electric fields in the in vivo human brain during transcranial electric stimulation. *Elife*. 2017;6:e18834. doi:10.7554/eLife.18834

24. Bortoletto M, Rodella C, Salvador R, Miranda PC, Miniussi C. Reduced current spread by concentric electrodes in transcranial electrical stimulation (tES). *Brain Stimul*. 2016;9(4):525-528. doi:10.1016/j.brs.2016.03.001

25. Mielczarek M, Olszewski J. Direct current stimulation of the ear in tinnitus treatment: a double-blind placebo-controlled study. *Eur Arch Oto-Rhino-Laryngology*. 2014;271(6):1815-1822. doi:10.1007/s00405-013-2849-6

26. Zeng F-G, Richardson ML, Tran P, Lin H, Djalilian H. Tinnitus Treatment Using Noninvasive and Minimally Invasive Electric Stimulation: Experimental Design and Feasibility. *Trends Hear*. 2019;23:1-12. doi:10.1177/2331216518821449

27. Grossman N, Bono D, Dedic N, et al. Noninvasive deep brain stimulation via temporally interfering electric fields. *Cell*. 2017;169(6):1029-1041.e16. doi:10.1016/j.cell.2017.05.024

28. Vöröslakos M, Takeuchi Y, Brinyiczki K, et al. Direct effects of transcranial electric stimulation on brain circuits in rats and humans. *Nat Commun*. 2018;9(1):483. doi:10.1038/s41467-018-02928-3

29. Mens LHM. Advances in Cochlear Implant Telemetry: Evoked Neural Responses, Electrical Field Imaging, and Technical Integrity. *Trends Amplif*. 2007;11(3):143-159. doi:10.1177/1084713807304362

30. Zeng F-G, Rebscher S, Harrison W, Sun X, Feng H. Cochlear Implants: System Design, Integration, and Evaluation. *IEEE Rev Biomed Eng*. 2008;1:115-142. doi:10.1109/rbme.2008.2008250

31. Vanpoucke FJ, Zarowski AJ, Peeters SA. Identification of the Impedance Model of an Implanted Cochlear Prosthesis From Intracochlear Potential Measurements. *IEEE Trans Biomed Eng*. 2004;51(12):2174-2183. doi:10.1109/tbme.2004.836518

32. Christopher P. Current flow patterns generated by cochlear implants. In: *Department of Biomedical Engineering*. Chapel Hill: The University of North Carolina; 2007.

33. Vandali AE, Sucher C, Tsang DJ, McKay CM, Chew JWD, McDermott HJ. Pitch ranking ability of cochlear implant recipients: A comparison of sound-processing strategies. *J Acoust Soc Am*. 2005;117(5):3126-3138. doi:10.1121/1.1874632

34. Tang Q, Benítez R, Zeng F-G. Spatial channel interactions in cochlear implants. *J Neural*

Eng. 2011;8(4):046029. doi:10.1088/1741-2560/8/4/046029

35. Zhu Z, Tang Q, Zeng F-G, Guan T, Ye D. Cochlear-implant spatial selectivity with monopolar, bipolar and tripolar stimulation. *Hear Res*. 2012;283(1-2):45-58. doi:10.1016/j.heares.2011.11.005

36. Duan YY, Clark GM, Cowan RSC. A study of intra-cochlear electrodes and tissue interface by electrochemical impedance methods in vivo. *Biomaterials*. 2004;25(17):3813-3828. doi:10.1016/j.biomaterials.2003.09.107

37. Bossetti CA, Birdno MJ, Grill WM. Analysis of the quasi-static approximation for calculating potentials generated by neural stimulation. *J Neural Eng*. 2008;5(1):44-53. doi:10.1088/1741-2560/5/1/005

38. Tran P, Sue A, Wong PCH, Li Q, Carter PM. Development of HEATHER for cochlear implant stimulation using a new modeling workflow. *IEEE Trans Biomed Eng*. 2015;62(2):728-735.

39. Nisancioğlu K, Newman J. The Transient Response of a Disk Electrode with Controlled Potential. *J Electrochem Soc*. 2007;120(10):1356. doi:10.1149/1.2403261

40. Sue A. *Electrochemical Safety Studies of Cochlear Implant Electrodes Using the Finite Element Method*. Sydney, Australia: The University of Sydney; 2016.

41. Tykocinski M, Duan YY, Tabor B, Cowan RSC. Chronic electrical stimulation of the auditory nerve using high surface area (HiQ) platinum electrodes. *Hear Res*. 2001;159(1-2):53-68. doi:10.1016/S0378-5955(01)00320-3

42. Shannon R V. A Model of Safe Levels for Electrical Stimulation. *IEEE Trans Biomed*

Eng. 1992;39(4):424-426.

43. Undurraga JA, Carlyon RP, Macherey O, Wouters J, van Wieringen A. Spread of excitation varies for different electrical pulse shapes and stimulation modes in cochlear implants. *Hear Res*. 2012;290(1-2):21-36. doi:10.1016/j.heares.2012.05.003

44. van den Honert C, Stypulkowski PH. Single fiber mapping of spatial excitation patterns in the electrically stimulated auditory nerve. *Hear Res*. 1987;29(2-3):195-206. doi:10.1016/0378-5955(87)90167-5

45. Rush S, Driscoll DA. Current distribution in the brain from surface electrodes. *Anesth Analg*. 1968;47(6):717-723.

46. Datta A, Bansal V, Diaz J, Patel J, Reato D, Bikson M. Gyri-precise head model of transcranial direct current stimulation: improved spatial focality using a ring electrode versus conventional rectangular pad. *Brain Stimul*. 2009;2(4):201-207.e1. doi:10.1016/j.brs.2009.03.005

47. Opitz A, Paulus W, Will S, Antunes A, Thielscher A. Determinants of the electric field during transcranial direct current stimulation. *Neuroimage*. 2015;109:140-150. doi:10.1016/j.neuroimage.2015.01.033

48. Carnevale NT, Hines ML. The NEURON Simulation Environment. *Neural Comput*. 1997;9(6):1179-1209.

49. Grant PF, Lowery MM. Electric field distribution in a finite-volume head model of deep brain stimulation. *Med Eng Phys*. 2009;31(9):1095-1103. doi:10.1016/j.medengphy.2009.07.006

50. Zhang TC, Grill WM. Modeling deep brain stimulation: point source approximation versus realistic representation of the electrode. *J Neural Eng*. 2010;7(6):1-11. doi:10.1088/1741-2560/7/6/066009

51. Mourdoukoutas AP, Truong DQ, Adair DK, Simon BJ, Bikson M. High-Resolution Multi-Scale Computational Model for Non-Invasive Cervical Vagus Nerve Stimulation. *Neuromodulation Technol Neural Interface*. 2018;21(3):261-268. doi:10.1111/ner.12706

52. Mielczarek M, Norena A, Schlee W, Olszewski J. Excitation of the auditory system as a result of non-invasive extra-cochlear stimulation in normal subjects and tinnitus patients. *Front Neurosci*. 2018;12(MAR):146. doi:10.3389/fnins.2018.00146

53. Joos K, de Ridder D, van de Heyning P, Vanneste S. Polarity specific suppression effects of transcranial direct current stimulation for tinnitus. *Neural Plast*. 2014;2014:1-8. doi:10.1155/2014/930860